Pulsar Radio Emission from Closed Field Lines Near Light Cylinder

Bi-Ping Gong*

The pulsar radio emission mechanism remains an enigma over half a century. A successful radiation process requires not only to explain the coherency, but also microstructures, characteristic frequency of emission, and the "death line" problem, etc. These challenge both the long standing gap models and recent models of magnetic reconnection with emission based on open field lines. This article points out that each intermittent plasma ejection from Y-point, the boundary of closed zone intersecting the equatorial plane, near the light cylinder of pulsar magnetosphere can stretch a bundle of closed field lines significantly. Corresponding magnetic pressure imposed on the trapped plasma provides ideal site of magnetic reconnection and hence generating pairs and Alfven wave near light cylinder. The resultant marginal stable instability is expected for coherent curvature emission. This not only interprets above problems in a simple and unified way, but also offers hints to the behavior of Rotating Radio Transients (RRATs) and Fast Radio Bursts (FRBs).

I. INTRODUCTION

The bright radio pulse requires a coherent emission of in phased charges accelerated by the pulsar, so that N charges radiating N^2 times the power in spontaneous emission per single charge.

There are two major coherence mechanisms: maser and antenna mechanisms. The most discussed antenna mechanism is coherent curvature emission (CCE), with a bunch either postulated as an initial condition or attributed to some physical process unrelated to curvature emission, such as soliton formation[1–4]. And how to achieve the negative absorption required in maser mechanism is still an open question[5].

All of these models require a certain kind of plasma instability, fast enough to create the bunches and to maintain their shape for sufficiently long times, which no mechanism can provide [5].

On the other hand, the global solution for magnetospheres is obtained using various numerical techniques [6–9]. In particular, it was found that time-dependent evolution generally leads to a solution with the Y-point localized near the light cylinder, where the boundary of closed zone intersects the equatorial plane on a circle of radius, R_Y [10].

The global kinetic plasma simulation of an axisymmetric pulsar magnetosphere using the particle-in-cell method can give rise to pair creation in a young pulsar far from the death line[11]. Neglecting the accumulation of toroidal field, B_ϕ, it shows: The energy release and e^+e^- creation are strongly concentrated in the thin, Y-shaped current sheet, with a peak localized in a small volume at the Y-point. The Y-point is shifted inward from the light cylinder by $\sim 15\%$ and "breathes" with a small amplitude. And gamma-ray emission peaks at the Y-point and is collimated in the azimuthal direction, tangent to the Y-point circle[11].

In contrast, taking into account of twisting of toroidal field, results in a toroidal magnetic field, B_ϕ, builds up on the closed field lines connected to the sheared cap[8]. The increased magnetic pressure in the closed zone causes these field lines to expand outwards. The expansion rate increases while the twist ψ grows with constant rate ω, and eventually the field lines expand through the light cylinder; this sets up a pattern of magnetospheric "breathing," where the amount of open flux oscillates, via reconnection in the current sheet, so that abrupt increase of spin period, occurring in giant flare of SGR 1900+14 can be interpreted[8]. No matter toroidal field built up or not [8, 11], the scenario of emission from current sheet trapped in opening field lines cannot give rise to radio emission of normal pulsars.

There are common observational challenges to both models of CCE at polar gap and radiation from reconnection at outer magnetosphere, i.e., pulsar radiation in over 5 orders of magnitude in rotation period and 6 orders of magnitude in B-field, producing more or less similar emission characteristics, over a very broad-band emission from $\sim$ 10MHz-100 GHz. In particular, the discovery of a highly magnetized, 75.88 s period, radio-emitting neutron star, PSR J0901-4046, located beyond the "death line" as defined by[2, 12], challenges both the polar cap models demanding a sufficient electric field parallel to B-field; and the reconnection induced radiation requiring strong light cylinder B-field [13].

Furthermore, recent observations show that a pulse profile actually build up a large number of localized, transient events, which are described as: intermittency, fine structures, discrete emissions, short-lived emission centers, microstructure and nanoshots[14]. Such a microstructure is too rapid to be caused by propagation through turbulence in i.e., the Crab nebula or in the interstellar medium[15], which becomes more severe in the case of nanobursts[16]. Those bright nanobursts must be coherent, radiating in characteristic emission frequency, and then passing through a highly transparent medium to avoid being thermalized[17]. The association of such microstructure with characteristic frequency and coherency may provide clue to the origin of CCE.

* Also at Department of Physics, Huazhong University of Science and Technology

Although extensive simulations on Y-point of pulsar magnetosphere have been performed, an analysis of very essence of physics underlying the Y-point near the light cylinder is still necessary. This paper suggests that piling up and relaxation of toroidal magnetic field near the light cylinder, causes intermittent ejection of plasma cloud and hence stretching of closed field lines in the vicinity of the light cylinder. The resultant reconnection automatically provides seeds of instability expected by CCE, so that a number of difficulties of previous models of radio emission can be solved, i.e., intermittent ejection can account for microstructures exhibited in a single pulse. The arrangement is as follows.

In Section (II) the forces experienced by the Y-point is revisited, so that an ejector carrying the closed field line beyond the light cylinder must be stretched significantly.

In Section (III), the plasma trapped in extremely stretched closed field line trigger rapid reconnection at the critical B-field generating electron-positron pair and Alfven wave (AW). In Section (IV), the ejected relativistic particles in phase with AW drift along the flux tube of open field lines giving rise to coherent curvature emission responsible for observation. Section (V) discusses circuit closure. Section (VI) applies the dynamo model to various pulsars, RRATs and FRBs.

All those processes occur near the light cylinder much shorter than R_{lc}, rather than extension to several light cylinder radius as shown in simulation, i.e.,[18] .

II. THE EFFECT OF CLOSED FIELD LINE AROUND THE LIGHT CYLINDER

Deviating from simulations with gamma-ray emission or radio emission of young pulsars based on reconnection occurring in opening field lines region, the closed field lines carried by plasma cloud ejected from Y-point is automatically stretched via magnetic tension providing ideal site of reconnection near the light cylinder.

Analogous to the solar dynamo with energy relaxation in oscillation between toroidal and poloidal field, the interaction of global helicity density and local dissipation of the pulsar magnetosphere can proceed in marginal stable state responsible for radio emission of pulsars.

The physics of the Y-point where the energy release and e^+e^- creation are peaked in a small volume, can be analyzed by the equation of motion of magnetohydrostatics,

$$\rho\frac{d\mathbf{v}}{dt} = \mathbf{J}\times\mathbf{B} + \rho_e\mathbf{E} \tag{1}$$

where $\mathbf{J}$ is the current density, ρ is the mass density, and $\rho_e = en_e$ is the charge density.

The Lorentz force F would vanish in Force Free Electrodynamics (FFE); however, it is nonzero in the dissipation region, passing the angular momentum from the electromagnetic field to the plasma. Neglecting ρE_ϕ (which would completely vanish in a true steady state), the azimuthal component of the Lorenz force, $F_\phi = -r\sin\theta[\rho_e E_\phi + (\mathbf{J}\times\mathbf{B})_\phi]$, can be rewritten [11],

$$F_\phi = |\mathbf{J_{pol}}\times\mathbf{B_{pol}}| = \mathbf{J_r}\mathbf{B_{pol}} = \mathbf{F}_\parallel$$

where J_r is the component of the electric current perpendicular to the magnetic flux surfaces. It is this component of $\mathbf{J}$ that creates torque per unit volume, $\ell = r\sin\phi F_\phi$, which creates torque at the Y-point accelerating charges of both signs in the positive ϕ-direction[11]. Energy is removed from the electromagnetic field and deposited into plasma in the case of $B_\phi = 0$ allowing Y-point shifting inward from the light cylinder by $\sim 15\%$.

In contrast, taking into account of piling up of toroidal field, B_ϕ, the expansion rate increases while the twist $\psi = \omega_0 t$ grows with constant rate ω, which can drive Y-point across R_{lc}. This sets up a pattern of magnetospheric "breathing," where the amount of open flux oscillates, via reconnection in the current sheet[8].

The current crossing the magnetic flux surfaces, requires a strong $J_\perp$, originating in B_ϕ, so that Equation (1) can be rewritten,

$$\rho|\frac{d\mathbf{v}}{dt}| = |\mathbf{J}\times\mathbf{B}| \approx \mathbf{J_r}\mathbf{B}_\theta + \mathbf{J}'_\theta\mathbf{B}'_\phi = \mathbf{F}_\parallel + \mathbf{F}'_\perp \tag{2}$$

where B'_ϕ and J'_θ are equivalence toroidal field and current density respectively.

When an intermittently ejection of plasma occurs at Y-point by $F_\perp$, it can carry a bundle of frozen closed field lines at time, t_0 at phase ϕ_0 to a hight ΔR beyond the light cylinder radius.

If such a cloud corotates to phase ϕ_1 at time t_1, by the pulsar spin, as shown in Fig1, it would result in a speed of cloud exceeding the speed of light, $(R_{lc}+\Delta R)\Omega > c$.

This can be avoided if only foot point of closed field line is carried from ϕ_0 to ϕ_1, while the cloud itself stays near ϕ_0 (or in an angle range of $\phi_0 < \phi < \phi_1$) at time t_1. In such a case, the closed field lines must be stretched, with a length, $\approx (\phi_1 - \phi_0)R_{lc}$, equivalent to a counter rotation speed of $\omega' \approx -\omega$, corresponding to a speed of $v_{am} \approx \omega' R_{lc} \approx c$ with respect to the comoving frame of the pulsar magnetosphere.

The trajectory of v_{am} based on closed field lines is a section of Archimedean spiral, $\Delta R = \beta\phi$, much shorter than that of open field line, with $\Delta R \ll R_{lc}$. Consequently, the cloud trapped in stretched closed field line leads to much stronger magnetic tension which provides a natural site of magnetic reconnection compared with that of open field line allowing a hight ΔR several time of R_{lc}, as shown in simulations i.e., [18].

The velocity of the ejector in the laboratory frame is read,

$$v = -\frac{(R_{lc}+\Delta R)(\phi_1 - \phi_0 + \Delta\phi_0)}{\Delta t} = -R_{lc}\Omega + v_{am} \tag{3}$$

where $v_{am} \approx -\Delta R\Omega - R_{lc}\Omega'$ corresponds to an equivalence velocity of a condensation in the comoving frame of pulsar magnetosphere, in which $\Omega = (\phi_1 - \phi_0)/\Delta t$ is the

spin speed of the star; and $\Omega' = \Delta\phi_0/\Delta t$ is the rotation speed of an ejector in the comoving frame of the pulsar magnetosphere, counter to the spin of the star.

The velocity of an ejector in the laboratory frame can be $v \approx 0$ or $|v| \ll c$ provided it travels at $v_{am} \approx c$ in the comoving frame of the pulsar magnetosphere, so that Equation (3) can be simplified as,

$$\frac{\Omega'}{\Omega} = -\frac{\Delta R}{R_{lc}} - 1 < 0 \tag{4}$$

Accordingly ejecting a distance of $\Delta R/R_{lc} \approx 1$ beyond the light cylinder (open field line case), the cloud is either decoupled from pulsar rotation, or required to rotate at a speed of $\Omega'/\Omega \approx -2$ counter to that of pulsar spin, otherwise the velocity of laboratory frame would exceed the speed of light, $v > c$.

In contrast, for an ejector carrying a bundle of closed field lines, it is much easier to achieve: $\Delta R/R_{lc} \ll 1$ and $\Omega'/\Omega \approx -1$. Because as soon as the cloud is ejected out by $F_\perp$, the corresponding closed field line is stretched by $F_\parallel$, which forms a section of Archimedean spiral.

Once the ratio of thickness to length of such a closed field line is stretched to $\delta/l \leq 1\%$, it gets reconnected [19]. Therefore, both the length of the closed field line itself and the jump hight of the ejector, ΔR are much less than R_{lc}.

In the case of giant flare occurring in magnetar, accumulated toroidal field B_ϕ can invoke a large drive force $F_\perp$, so that the closed field lines can be ejected to larger distance ΔR beyond R_{lc} than those of normal pulsars with relatively smaller ΔR beyond R_{lc}, even inside R_{lc}.

III. THE CRITICAL B-FIELD, RECONNECTION AND SEED OF CCE

The breath of the Y-point in the vicinity of R_{lc} is determined primarily by piling up and dissipation of the toroidal field. For a normal radio pulsar the amplitude of breath is small so that the ejection of cloud by $F_\perp$, and stretching of corresponding closed field line by $F_\parallel$ can proceed in a marginal stable state, offering an ideal site of reconnection and hence ingredient required by CCE.

The motion of an ejector of speed, $v_{am} \sim c$, is resisted by the magnetic force of the closed field line as shown in Equation (1), which reduces to the magnetic tension, $\mathbf{J}\times\mathbf{B} = \frac{B^2}{\mu}\frac{\mathbf{n}}{R_c}$, where $\mathbf{n}$ is the principle normal, R_c is the radius of curvature, and μ is the magnetic permeability.

Such a magnetic tension enhances significantly by concentrating plasma and closed field lines in the narrow equatorial layer, occurring near the light cylinder.

The ejection of a cloud out of Y-point results in stretching of corresponding closed field line via motion of foot point of closed field line as shown in Equation (3). This is equivalent to plunging of an ejector into the closed field line with velocity, $v_{am} \sim c$, which stretches and compress the closed field line to a narrow shape resulting in reconnection. Such a process resembles the experiment[20], in which a weak-external B-field in the direction perpendicular to the plasma propagation is applied, where the B-field is directly coupled with electrons. Since the kinetic pressure of plasma is much larger than the magnetic pressure, the B-field is distorted and locally anti-parallel. Plasma collimations, cusp and plasmoid like features with optical diagnostics are reported. Moreover, the plasmoid propagates at the electron Alfven velocity, indicating a reconnection driven by the electron dynamics [20]. The configuration of B-field is also similar to the solar wind induced ballooning instability in the near-Earth plasma sheet responsible for the onset of a substorm expansion through reconnection [21].

The balance of kinetic energy and magnetic tension is equivalent to the balance between the magnetic energy density and the kinetic energy density in the reconnection zone, so that the energy release at the critical B-field, B_T, corresponds to an energy density of,

$$\frac{B_T^2}{\mu} \sim \rho c^2 \sim n_e \gamma m_e c^2. \tag{5}$$

where the critical B-field range from $B_T \sim 10^5$T, for young pulsars like the Crab pulsar, and $B_T \sim 10^3$T for relative old pulsars. While the critical field for normal pulsars is $B_T \sim 10^4$T, which corresponds to an electric field, $E \sim cB_T \sim 3\times 10^{12} V/m$, sufficient not only producing pairs of energy level, $\sim 2m_e c^2$ (m_e is the electron mass), but also accelerating pairs of a number density of $n_e \sim 10^{24} m^{-3}$ to relativistic speed of Lorentz factor, $\gamma \sim 10^2$.

As a result, a small volume, V_{rec}, formed by stretched closed field lines is ejected from the volume, V, of Y-point with number density of n_Y, so that a much higher number density, $n_e \sim n_Y V/V_{rec}$, is expected at the reconnection site.

The number density of Equation (5) corresponds to a flow of charged particles through the reconnection zone as shown in Fig1c,

$$n_e \approx \frac{J_r}{e v_r} \tag{6}$$

where v_r is the speed of charged particles corresponding to the current, $J_r = \frac{1}{\mu}\frac{dB_\phi}{dr} \sim \frac{2B_T}{\mu\delta}$ (where δ is the thickness of the current layer) in the spherical coordinate system as shown in Fig1a.

The narrow tip of the last closed field lines originating in magnetic tension as shown in Fig1c, can drift at the speed of light, $v_{am} \sim c$. Because transferring magnetic energy piled up at the Y-point with a volume of $V \sim 2L_l L_b L_\delta$; to a narrow layer of volume, $V_{rec} \sim \delta b l$, yields a speed of plasma in the narrow region of, $v_\phi \sim v_{am} \sim c$, by the mass conservation of the Sweet-Parker layer, $v_\theta L_l \sim v_\phi \delta$ as shown in Fig1a.

The speed $v_{am} \sim c$ in comoving frame corresponds to a laboratory speed at tip of last closed field line of $v = 0$ near the light cylinder, which is actually required in observation. Since it is only in such a circumstance

that subsequent emission site is approximately at rest to the observer. Otherwise, i.e., a laboratory velocity of of $v = -c$ (correspond to $v_{am} \sim 0$) would suffer from severe Doppler deboosting which weak the brightness of emission profoundly.

Moreover, the speed $v_{am} \sim c$ at vicinity of R_{lc} is required by the limit of stretching closed field line. Substituting the number density of Equation (6) into Equation (5), the critical B-field of $B_T \sim 10^4$T can be achieved by,

$$B_T \approx \frac{\gamma}{v_r \delta} \frac{2 m_e c^2}{e} \approx \frac{\gamma}{v_r \delta} 10^6 \tag{7}$$

In other words, only when the tip of last closed field lines is stretched to a thickness of $\delta \sim 10^{-2} m$ at the vicinity of R_{lc}, can the critical field of, $B_T \sim 10^4$T, be reached at the reconnection zone, in which case, a speed of plasma $v_r \sim 10^6 m/s$ and a much larger speed of v_ϕ of Lorentz factor, $\gamma \sim 10^2$, are expected as shown in Fig1bc.

On the other hand, the magnetic diffusion at the critical B-field, B_T, also gives rise to a AW propagating along the field lines, which can be investigated simply by the combination of equation of induction,

$$\frac{\partial \mathbf{B}}{\partial t} = \nabla \times (\mathbf{v} \times \mathbf{B_0}) + \eta \nabla^{\mathbf{2}} \mathbf{B} \tag{8}$$

and equation of motion of Equation (1) simplified as $\rho \frac{d\mathbf{v}}{dt} = \mathbf{j} \times \mathbf{B_0}$. Such a diffusion can proceed in a marginal stable state with the magnetic diffusivity, η; and the background B-field at the reconnection site satisfying $B_0 \approx B_T$.

Under the usual wave assumption, $exp(-\omega_i t) exp(i\omega_r t)$, a simple dissipation relation is obtained[22],

$$\omega^2 = k^2 v_A^2 - i\omega \frac{k v_A}{R_m}, \tag{9}$$

where v_A is the Alfven speed, $R_m \equiv L v_A / \eta$ is the magnetic Reynolds number, and L is the length of current sheet at the reconnection site.

The current sheet formed by trapped plasma can be fragmented into a chain of rapidly growing secondary magnetic islands or plasmoids, with the smallest elementary current sheets, of size δ, as shown in Equation (7), so that the equivalent length of current sheet becomes $L \approx \delta$ in Equation (9).

A distribution of such a relativistic particles interact with a distribution of waves leading to the sloshing about of particles in the waves, and resonant wave-particle interactions[22, 23]. Therefore, once a plasmoid gets reconnected at the apex of the last closed fields, the magnetic Reynolds number of Equation (9) becomes $R_m \sim v_A \delta / \eta$.

Splitting ω of Equation (9) into a real ω_r and imaginary ω_i, the wave frequency, $\omega_r \approx k v_A$, corresponds to a time scale of,

$$\tau_r = \frac{2\pi}{\omega_r} \sim 2\pi (\frac{\lambda}{1 \times 10^{-2}}) (\frac{3 \times 10^8}{v_A}) \sim 2 \times 10^{-10} s \tag{10}$$

And the damping of such an AW is determined by $\omega_i = -k v_A / (2 R_m)$, where $R_m \sim 10^{-6}$ in the case of $\eta \sim 1 m^2/s$. As a result, one gets,

$$\tau_i = \frac{2\pi}{\omega_i} \sim 2\pi \mu_0 (\frac{\lambda}{1 \times 10^{-2}})^2 (\frac{1}{\eta}) \sim 8 \times 10^{-10} s \tag{11}$$

Consequently, Equation (10) and Equation (11) predict a wave train of length, $s \sim \tau_i c \sim 2 \times 10^{-1}$m, a wave number of, $k \sim 1/\delta \sim 10^2$, and hence, $ks \sim 20 \gg 1$, which corresponds to a GHz nanoburst of short frequency range, $\Delta\omega/\omega = (\omega_r^2 - \omega_i^2)^{1/2} / \omega_r \approx 0.03$, comparable to a typical FRB.

The reconnection determined by Equation (10) and Equation (11) alway takes place at the apex of the last closed field lines which can be achieved by a new last closed field line denoted by (2) catching up the old one (1) as shown in Fig1a.

The duration of a microstructure is much shorter than a nanoburst is constrained by both the characteristic frequency of GHz and the coherent condition, $ks \gg 1$. Therefore, the characteristic frequency of GHz, nanoburst, the critical B-field, as well as pair production as shown in Equation (7) are closely related in the context of reconnection induced radio emission.

The particles and waves stemming from the magnetic reconnection at the critical field, B_T, can undergo resonant wave-particle interaction,

$$\omega - \mathbf{k} \cdot \mathbf{v} = \mathbf{0}, \tag{12}$$

in an unmagnetized plasma, which can be achieved as beam of particles and AW propagating along the center of the flux tube formed by the open field lines, where the strength of B-field approximately canceled out as shown in Fig1b.

IV. CCE

A bunch in phase with AW interacting with curved field lines gives rise to CCE naturally. The energy radiated per unit solid angle per unit frequency interval from a bunch with volume V and number of $N_e \sim n_e V$ particles drifting along a curved field line[24],

$$\frac{dI_{tot}}{d\omega d\Omega} = \frac{dI}{d\omega d\Omega} F_\omega(N_e) \tag{13}$$

where $F_\omega(N_e)$ is a dimensionless parameter denoting the enhancement factor due to coherence defined,

$$F_\omega(N) = |\Sigma_j^N e^{-i\omega(\mathbf{n} \cdot \Delta \mathbf{r}_j / c)}|^2 \tag{14}$$

where, $\mathbf{n}$, is the unit vector to the observer, and $\Delta \mathbf{r}_j$ is a section of the bunch length L_{bc}. The emission of such a bunch could be coherent only if all such small sections are in phase, with each small section of size $\Delta r_j \ll \lambda$. The fast variability and stability required in generation

of such a phase relationship is difficult to achieve in the usual bunch models.

While the reconnection induced pairs and AW, with resonant wave-particle interactions automatically gives rise a bunch of coherent length responsible for coherent emission. Because it allows the growth or damping of wave, and the scattering and acceleration of particles, so that the particle sees the electric field of wave as static fielding its rest frame[22].

As a result, an AW of wave length, $\lambda \sim 1\times10^{-2}$m, and a coherent length $c\tau_i \sim 20\lambda$ corresponds to a coherent bunch of length comparable to that of the wave train, $L_{bc} \sim \sum \Delta r_j \sim 20\lambda$. Then simply applying the half wave superposition, the enhancement factor of such an in phased bunch becomes $F_\omega(N_e) = N_e^2$, responsible for the emission of a coherent nanoburst.

The fast reconnection of a plasmoid occurring at the apex of the last closed field lines produce a nanoburst as shown in Fig1a. Such a process is replaced by a new last closed field lines and a new nanoburst... The swing of those nanobursts through a pulse window results in the single pulse of a pulsar, with an enhancement factor of Equation (14) of,

$$F_\omega(N_e, N) = \Sigma_1^N N_e^2 \tag{15}$$

where N_e and N are the number of particles in a nanoburst and the number of nanoshots in a single pulse respectively. This explains why the single pulse of a pulsar appears much dimmer than a nanoburst.

Therefore, it also provides a concrete mechanism to the speculation[16] that: microbursts are incoherent superpositions of short-lived narrowband, nanoshots, and all microbursts are clumps of nanoshots. In such a case, the broadband of each microburst can be interpreted by widening the frequency range of the centre frequencies of the nanoshots (each with a very short frequency range as shown under Equation (11)) in a microburst[16].

Accumulation of B-field to the critical level, B_T, near the light cylinder can invoke rapid magnetic reconnection well accounting for coherency, microstructure, characteristic frequency of GHz of radio emission of pulsars.

To allow the AW propagate through plamoids, the plasma frequency must be lower than that of the characteristic frequency of 1GHz,

$$\omega_p = (\frac{4\pi n_e e^2}{m_e})^{1/2} \lesssim \omega_A \sim 1GHz. \tag{16}$$

which in turn demands, $n_e \lesssim 3\times10^{24}m^{-3}$. Notice the plasma frequency above is much greater than the cyclotron frequency, $\omega_p \gg \omega_{cy} \approx eB_T/(m_e c) \approx 10^7$Hz. Substituting the above limit on particle density into the constraint of Equation (5), the Lorentz factor is required to be $\gamma \gtrsim 3\times10^2$. In other words, the energy dissipation through reconnection at the critical B-field, B_T, can both produce and accelerate pairs of number density of $n_e \lesssim 3\times10^{24}m^{-3}$ to relativistic speed of Lorentz factor, $\gamma \gtrsim 3\times10^2$, which forms a coherent bunch resulting in coherent curvature emission through subsequent interaction with the flux tube formed by open field lines.

Pairs ejected from the reconnection site drift along a flux tube formed by open field lines as shown in Fig1 at speed $v_{am} \sim c$ in the rest frame of the pulsar magnetosphere, such relativistic plasma can give rise to curvature radiation of effective frequency of

$$\nu = \frac{\gamma^3 c}{\rho} \sim 1GHz \tag{17}$$

which corresponds to a power of coherent curvature radiation[25] ,

$$P_{cv} = \frac{N_e^2 e^2 c\gamma^4}{\rho^2} \tag{18}$$

where $N_e = n_e V$ is the number of charged particles contained in a bunch of volume, V. It is worth mention that the velocity of the emission site is $v \approx v_{am} - \Omega R_{lc} \approx 0$ in the laboratory frame.

The interacting of the coherent bunch of length, $L_{ch} \sim 20\lambda$ with open B-field line of curvature radius, $\rho \sim R_{lc}$, corresponds to a spread angle of, $\phi \sim L_{ch}/R_{lc} \sim 10^{-8}$, the misalignment angle between the front and end of a bunch emitting radio waves tangentially to the field lines, which is much less than the angle of emission cone, $1/\gamma \sim 10^{-2}$ with $\gamma \sim 100$ denoting the Lorentz factor of plasma. Consequently, the coherency of each nanoburst is ensured, while different nanobursts can be incoherent as they swing through the line of sight.

Moreover, previous bunch models suffer from other problems such as: the growth of the instability is not fast enough; and velocity dispersion resulted random-phase rather than phase coherent ones[23]. Again the new scenario provides both fast instability and limited velocity dispersion. Because the reconnection occurred at the apex of last closed field lines with a layer thickness, $\delta \sim 10^{-2}$m, automatically gives rise to a fast instability of frequency of GHz.

Furthermore, limited frequency dispersion of AW as shown in Equation (10) and Equation (11) corresponds to a limited velocity dispersion of particles under the resonant particle-wave interaction. Therefore, the problems of coherent emission by bunch can be avoided in the new scenario.

On the other hand, as the reconnection always takes place at the apex of last closed field line, the subsequent radiation can propagate in the flux tube of open field lines with much lower particle density than that inside the current layer. Such a "density cavity" like environment deviates from models of reconnection by coalescence of magnetic islands in the current sheet, where magnetic perturbations should propagate in the dense current sheet[13].

V. CIRCUIT CLOSURE

The reconnection zone corresponds to a reconnection electrical field accelerating plasma to relativistic speed

near X line as shown in Fig1b. The presence of guided field in the X line region of the reconnection site leads to strongly field aligned distribution of beams of electron and positron[26]. One pair of electron and positron return to the pulsar surface directly along separatrices of the X line, as shown in Fig1b, and the other pair of energetic electron and positron beams move along opposite pair of separatrices of the X line away from the pulsar, giving rise to coherent radiation and eventually contributing to the pulsar wind.

In the new scenario, the so called "trapped disc charge" [17, 27] is driven to the light cylinder triggering magnetic reconnection and generating pair production. The resultant return plasma drifting along the separatrices to the pulsar surface as shown in bottom of Fig1b.

The charge neutrality of the pulsar is ensured, as long as the outward loss of negative charge at domes toward the pulsar wind is equivalent to the positive disc charge driven to the reconnection site as shown in Fig1b; Furthermore, the return electrons and positrons are approximately charge neutral. This automatically results in a marginal stable circuit of the pulsar magnetosphere as shown in Fig1d.

The circuit stemming from dynamo process in magnetosphere is compatible with numerical simulations which exhibit that pair production can be triggered in the diffusing region, where half return to the pulsar surface along separatrices, and other half plasma eject out contributing to the pulsar wind[28].

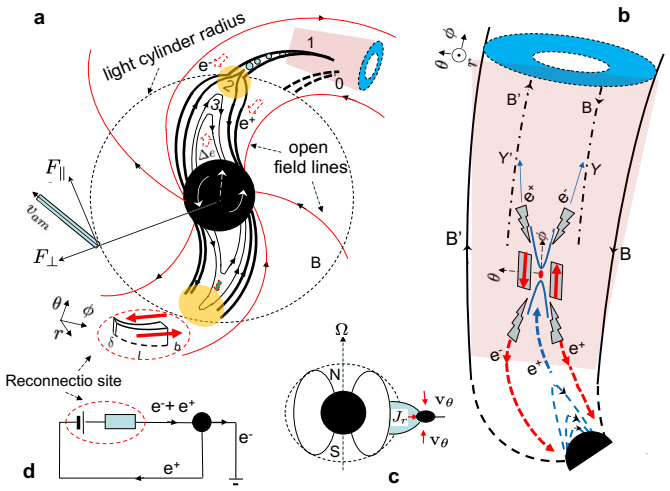

FIG. 1. A schematic configuration of the dynamo magnetosphere. Panel a: pulsar spin deformed last closed field lines surrounded by flux tube of open field lines. The two thin reconnection layers at top (with plasmoids inside) and bottom provide sites of reconnection giving rise to beams and waves, Panel b: reconnection site with guided field which separates the electron and positron beams. The outward beams interact with the open field lines invoking coherent emission Panel c: side view of Y-point jointing closed zone with the equatorial sheet, where pressure from θ direction and radial current are imposed. Panel d: the reconnection zone: (i) provides the return electrons and positrons; and (ii) supplies positrons of the dome-disc charge from the closed field lines, (iii) the loss of charged particles to pulsar wind is equivalent to grounding in circuit. Finally a closure circuit is achieved.

VI. GLOBAL-LOCAL INTERACTION AND APPLICATION TO PULSARS AND FRBS

Based on CCE produced in previous sections, the energy budget and resultant intermittency, as well as frequency-width relation and trombone phenomena occurring in various pulsars and FRBs will be discussed.

A. The Crab pulsar and PSR J0437-4715

For young pulsars, i.e., Crab pulsar with spin period $P = 33ms$, its surface and light-cylinder B-field are, $B_s \approx 4\times10^8$T and $B_{lc} \approx 1\times10^2$T respectively. The accumulation of B-field to the critical value, $B_T \sim 10^5$T, at the reconnection zone takes two steps.

Firstly, piling up of B-field at Y-point corresponds to a magnetic energy of $E_H = B_\phi^2 V/\mu$, where $V \sim 2L_\delta L_b L_l$ denoting the volume of Y-point as shown in Fig1ac.

In the case of a Y-point of length, thickness and width, $L_l \sim L_\delta \sim L_b \sim 10^{-3}R_{lc} \sim 4\times10^3$m, the magnetic energy pile up at Y-point is read,

$$E_H \sim 2\times10^6(\frac{B_\phi}{3\times10^3})^2(\frac{L_\delta}{4\times10^3})(\frac{L_b}{4\times10^3})(\frac{L_l}{4\times10^3}) \sim 10^{22}J \quad (19)$$

Transferring the energy of Equation (19) into the reconnection site is equivalent to plasma beams flowing from the Y-point of a large volume, V, into the reconnection region of small volume, $V_{rec} \sim \delta bl$. The suppression of the Y-point of length L_l with velocity, v_θ, into the Sweet-Parker layer of thickness, δ and velocity, $v_\phi \sim c$, requires,

$$(\frac{v_\theta}{10^3})(\frac{L_l}{10^3}) \approx (\frac{v_\phi}{10^8})(\frac{\delta}{10^{-2}}) \quad (20)$$

which corresponds to a time scale of energy release of, $\tau \sim L_l/v_\theta \sim 1s$. If Y-point B-field required in energy piling up of Equation (19), $B_\phi \sim \psi B_{lc} \approx 30B_{lc} \approx 3\times10^3$T, equals the time scale of energy release, $\tau \sim \psi/\omega \sim 1s$, a corresponding rate of piling up of toroidal field is expected $\omega \sim 30s^{-1}$.

The ejection of plasma cloud near the light cylinder leads further enhancement of B-field by bending and concentration of closed field lines at the reconnection zone, so that the critical field is reached for such a young pulsar, $B_T \sim 30B_\phi \sim 10^5$T. With a magnetic Reynolds of $R_m \sim v_A\delta/\eta$ at the reconnection zone, a rapid reconnection occurs of power of $P_R = \frac{B_T^2}{\mu}\delta b v_\phi$,

$$P_R \sim 10^6(\frac{B_T}{10^5})^2(\frac{\delta}{10^{-2}})(\frac{b}{10^0})(\frac{v_\phi}{10^8}) \sim 10^{22}W \quad (21)$$

where $v_\phi \sim c$ is the drifting speed of plasma at the dissipation region observed at the rest frame of the spinning pulsar. While in the laboratory frame such a drifting velocity becomes, $v \approx v_\phi - \Omega R_{lc} \approx 0$.

The energy budget of the oscillation of piling up and relaxation of magnetic energy of Equation (19) and Equation (21) can be estimated as,

$$\dot{E}_H \approx \frac{E_H}{\tau} \approx P_R, \tag{22}$$

For pulsars like the Crab pulsar the time scale of such an oscillation can be as short as $\sim$ 1s.

In fact, the radiation power of Equation (21) is compatible with radio emission of the Crab pulsar[29], which corresponds to a very small fraction (typically 10^{-6} to 10^{-5}) of the total energy loss of a pulsar.

The relativistic pairs ejected from the reconnection site drift along the flux tube formed by the open field lines which invoke curvature radiation with a curvature radius of $\rho \sim R_{lc}$. And considering the frequency constraint of Equation (17), and the Lorentz factor of $\gamma \sim 300$, the number density of charged particles, $n_e \sim 3 \times 10^{24} m^{-3}$ can be estimated.

The reconnection of a plasmoid proceeds in a small volume of $V_{rec} \sim \delta b l \sim 10^{-2} m^3$ at the apex of the last closed field line, giving rise to a power of coherent curvature radiation, $P_{cv} \sim 10^{17}$W by Equation (18). Furthermore, to consist with observational power of radio emission of the Crab pulsar[29], $P_{ob} \sim 10^{22}$W, a number of plasmoids of $N \sim 10^5$ need to be reconnected per second. Such a coherent curvature emission provides a sample of coherent emission as shown in Equation (15), in which the number of plasmoids and the number of particles in a plasmoid are respectively, $N \sim 10^5$ and $n_e \sim 10^{24} m^{-3}$. And such a number density in reconnection zone is consistent with that of Y-point, $n_e \sim n_Y V / V_{rec} \sim 10^{24} m^{-3}$ where $n_Y \sim \epsilon_0 \Omega B_\phi \sim 10^{12} m^{-3}$.

The millisecond pulsar, PSR J0437-4715 (spin period $P \approx 5.8 ms$), corresponds to a surface B-field of only $B_s \approx 6 \times 10^4$T, which is 4 order of magnitude less than that of the Crab pulsar. While the resultant energy, power of curvature radiation and energy budget of Equation (19)-Equation (22) are almost identical those of the Crab pulsar.

Consequently, similarities between the Crab pulsar and millisecond pulsars in radio emission which is difficult to understand in the context of polar cap models as well as magnetic reconnection at light cylinder magnetic, B_{lc}, can be well interpreted by the process of closed field lines near light cylinder.

B. PSR J0953+0755, PSR J0901-4046 and the death line problem

PSR J0953+0755 is a bright nonrecycled pulsar whose single-pulse fluence variability is reportedly large[30] . With period of $P \approx 0.253$s, a spindown age of 1.75×10^7yr, the surface and light curve B-field of this pulsar are $B_s \approx 2 \times 10^7$T and $B_{lc} \approx 1 \times 10^{-2}$T respectively.

Likewise, in the case of a Y-point of length, thickness and width, $L_l \sim L_\delta \sim L_b \sim 10^{-3} R_{lc} \sim 4 \times 10^6$m, and an enhanced B-field at Y-point, $B_\phi \sim 10^{-1}$T, corresponds to a magnetic energy of,

$$E_H \sim 2 \times 10^6 (\frac{B_\phi}{1 \times 10^{-1}})^2 (\frac{L_\delta}{4 \times 10^6})(\frac{L_b}{4 \times 10^6})(\frac{L_l}{4 \times 10^6}) \sim 10^{24} J \tag{23}$$

The suppression of the Y-point of length L_l with velocity, v_θ, into the Sweet-Parker layer of thickness, $\delta \sim 10^{-1} m$ and velocity, $v_\phi \sim c$, requires,

$$(\frac{v_\theta}{10^1})(\frac{L_l}{10^6}) \approx (\frac{v_\phi}{10^8})(\frac{\delta}{10^{-1}}) \tag{24}$$

Similarly, further enhancement of B-field by bending and concentration of closed field lines at the reconnection zone, results in a B-field of reconnection, $B_T \sim 10^4 B_\phi \sim 10^3$T and hence a power of

$$P_R \sim 10^6 (\frac{B_T}{10^3})^2 (\frac{\delta}{10^{-1}})(\frac{b}{10^0})(\frac{v_\phi}{10^8}) \sim 10^{19} W \tag{25}$$

The magnetic energy accumulation and relaxation of Equation (23)-Equation (25), corresponds to a twisting time of $\tau \sim L_l / v_\theta \sim 1/\omega \sim 10^5$s.

Such a magnetic energy piled up of PSR J0953+0755 can radiate at the observational power of radio emission[29], $P_R \sim P_{ob} \sim 10^{19}$W, for a time interval of $E_H / P_{ob} \sim 10^5$s, which is much longer than that of Crab pulsar.

Furthermore, the curvature radius $\rho \sim R_{lc} \sim 1 \times 10^9$m, and the constraint of Equation (17), requires a Lorentz factor of $\gamma \sim 900$ and a number density of charged particles, $n_e \sim 1 \times 10^{24} m^{-3}$, which corresponds to a power of curvature radiation of PSR J0953+0755, $P_{cv} \sim 5 \times 10^{12}$W. Therefore, in a pulse window of PSR J0953+0755 , it is required to reconnect a number of $N \sim 10^5$ plasmoids in order to comply with the observed power of $P_{ob} \sim 10^{19}$W[29].

The number density of PSR J0953+0755 in reconnection zone can consist with its Y-point density, $n_e \sim n_Y V / V_{rec} \sim 10^{24} m^{-3}$, in the case of $n_Y \sim 10^5 m^{-3}$.

PSR J0901-4046 locates beyond the "death line"[2, 12], and exhibits quasi-periodicity and partial nulling[31]. In the new scenario, the balance of energy budget and radiation properties of PSR J0901-4046, as well as corresponding parameters resemble those of PSR J0953+0755 as shown in Equation (23)-Equation (25), which also exhibits partial nulling[32].

C. Nonlinearity and Conclusion

The dissipation of Equation (22) does not alway proceed in marginal stable state with normal emission, i.e., on some days PSR J0953+0755 exhibits a large number of giant pulses, there are other days when it enters nulling

state with no detectable emission in the power spectrum or in the folded pulse data[32].

Interestingly, one of RRAT, neutron stars emitting sporadic radio bursts, RRAT J1913+1330, displays sequential pulse trains during active phases with significant pulse variations in profile, fluence, flux, and width, as well as between adjacent sequential pulses[33]. And repeat FRB 121102 exhibits 1,652 independent bursts with a peak burst rate of 122 per hour, in 59.5 hours spanning 47 days [34].

Such striking similarities indicate that normal pulsars, RRATs, and FRBs share common physics underlying them, the nonlinearity occurring the dynamo process of the pulsar magnetosphere provides a simple and natural candidate. In fact, the nonlinearity in the interaction between global magnetic energy and local dissipation has been studied extensively in astronomical objects.

A convenient approach is to investigate helicity density transport near the marginal state. When adding a small perturbation to the current sheet in the marginal state, the local current gradient will exceed the critical value, which leads to current sheet fragmentation or plasmoid formation[35, 36]. The evolution equation for magnetic helicity density is essentially based on the induction equation of Equation (8), which takes the form of the Burgers equation[35]. In such a case, helicity density transport near the marginal state is intermittent and episodic. And some detailed analysis[35] shows that there are indeed soliton-like solutions.

The energy conservation of Equation (22) and coherence of Equation (15) together yield,

$$E_H(t) \sim N_s(t)N(t)E_G(t) \tag{26}$$

where the energy release at left hand side is presented by the accumulation time scale by number of pulsar spins proportional to the accumulation of toroidal field, $N_s \propto \omega t$, which can dissipate in giant pulses of number of, $N_s N$, and fluence of giant pulse of E_G.

The marginal stable state can be reached by i.e., Crab pulsar, $N_s(t) \sim 30$, $N(t) \sim 10^5$, and $E_G(t) \sim 10^{40}$K. Deviation from such a marginal stable state corresponds to a time varying values of Equation (26) determined by nonlinearity of Equation (8), such that much brighter giant pulse, with fluence $E_G \gg 10^{40}$K resembling FRBs, can be achieved by accumulation of extra energy during marginal stable emission.

Likewise, normal and old pulsars, also have chance to emit intermittent and episodic giant pulses mimicing RRATs; or even much stronger giant pulses of fluence $E_G \gg 10^{40}$K responsible for FRBs at the cost of much longer twisting spins, $N_s(t)$, than that of young pulsars. This provides an explanation to the repeating FRB 20200120E found in an M81 globular cluster[37].

The ejected cloud by accumulated toroidal field results in stretched closed field line near light cylinder, which triggers rapid reconnection with a group of parameters, i.e., the critical B-field, size of reconnection zone, and charge density.

In such a scenario, the discrepancies in spin period for 5 order of magnitude, and strength of B-field for 6 order of magnitude among young and old pulsars are narrowed to 2 order of magnitude difference in the critical B-field, B_T, which naturally interpret the death line problem and the similarities between the Crab pulsar and the millisecond pulsar PSR J 0437-4715.

Consequently it account not only for theoretical problems: (1) pair production, (2) nanoshots, (3) CCE, (4) circuit closure, and (5) density cavity; but also observational problems: (a) death line problem, (b) character frequency of GHz, (c) intermittency of pulsars and FRBs. Many aspects of the new scenario await further investigation and observational test.

[1] P. A. Sturrock, A Model of Pulsars, The Astrophysical Journal **164**, 529 (1971).

[2] M. A. Ruderman and P. G. Sutherland, Theory of pulsars: polar gaps, sparks, and coherent microwave radiation., The Astrophysical Journal **196**, 51 (1975).

[3] G. Benford and R. Buschauer, Coherent pulsar radio radiation by antenna mechanisms: general theory., Monthly Notices of the Royal Astronomical Society **179**, 189 (1977).

[4] J. Gil, Y. Lyubarsky, and G. I. Melikidze, Curvature Radiation in Pulsar Magnetospheric Plasma, The Astrophysical Journal **600**, 872 (2004), arXiv:astro-ph/0310621 [astro-ph].

[5] D. B. Melrose, M. Z. Rafat, and A. Mastrano, Pulsar radio emission mechanisms: a critique, Monthly Notices of the Royal Astronomical Society **500**, 4530 (2021), arXiv:2006.15243 [astro-ph.HE].

[6] I. Contopoulos, D. Kazanas, and C. Fendt, The Axisymmetric Pulsar Magnetosphere, The Astrophysical Journal **511**, 351 (1999), arXiv:astro-ph/9903049 [astro-ph].

[7] A. Spitkovsky, Three-dimensional Pulsar Magnetosphere, in *AAS/High Energy Astrophysics Division #9*, AAS/High Energy Astrophysics Division, Vol. 9 (2006) p. 4.03.

[8] K. Parfrey, A. M. Beloborodov, and L. Hui, Twisting, Reconnecting Magnetospheres and Magnetar Spindown, The Astrophysical Journal Letters **754**, L12 (2012), arXiv:1201.3635 [astro-ph.HE].

[9] D. A. Uzdensky and A. Spitkovsky, Physical Conditions in the Reconnection Layer in Pulsar Magnetospheres, The Astrophysical Journal **780**, 3 (2014), arXiv:1210.3346 [astro-ph.HE].

[10] X.-N. Bai and A. Spitkovsky, Modeling of Gamma-ray Pulsar Light Curves Using the Force-free Magnetic Field, The Astrophysical Journal **715**, 1282 (2010), arXiv:0910.5741 [astro-ph.HE].

[11] R. Hu and A. M. Beloborodov, Axisymmetric Pulsar Magnetosphere Revisited, The Astrophysical Journal

939, 42 (2022), arXiv:2109.03935 [astro-ph.HE].
[12] K. Chen and M. Ruderman, Pulsar Death Lines and Death Valley, The Astrophysical Journal **402**, 264 (1993).
[13] Y. Lyubarsky, Radio emission of the Crab and Crab-like pulsars, Monthly Notices of the Royal Astronomical Society **483**, 1731 (2019), arXiv:1811.11122 [astro-ph.HE].
[14] D. Melrose, Pulse Emission Mechanisms, in *Young Neutron Stars and Their Environments*, Vol. 218, edited by F. Camilo and B. M. Gaensler (2004) p. 349, arXiv:astro-ph/0308471 [astro-ph].
[15] J. H. Crossley, J. A. Eilek, T. H. Hankins, and J. S. Kern, Short-lived Radio Bursts from the Crab Pulsar, The Astrophysical Journal **722**, 1908 (2010), arXiv:1009.0735 [astro-ph.HE].
[16] J. A. Eilek and T. H. Hankins, Radio emission physics in the Crab pulsar, Journal of Plasma Physics **82**, 635820302 (2016), arXiv:1604.02472 [astro-ph.HE].
[17] F. C. Michel and H. Li, Electrodynamics of neutron stars, Physics Reports **318**, 227 (1999).
[18] A. Philippov, D. A. Uzdensky, A. Spitkovsky, and B. Cerutti, Pulsar Radio Emission Mechanism: Radio Nanoshots as a Low-frequency Afterglow of Relativistic Magnetic Reconnection, The Astrophysical Journal Letters **876**, L6 (2019), arXiv:1902.07730 [astro-ph.HE].
[19] D. A. Uzdensky and A. Spitkovsky, Physical Conditions in the Reconnection Layer in Pulsar Magnetospheres, The Astrophysical Journal **780**, 3 (2014), arXiv:1210.3346 [astro-ph.HE].
[20] Y. Kuramitsu, T. Moritaka, Y. Sakawa, T. Morita, T. Sano, M. Koenig, C. D. Gregory, N. Woolsey, K. Tomita, H. Takabe, Y. L. Liu, S. H. Chen, S. Matsukiyo, and M. Hoshino, Magnetic reconnection driven by electron dynamics, Nature Communications **9**, 5109 (2018).
[21] P. Zhu and J. Raeder, Ballooning instability-induced plasmoid formation in near-Earth plasma sheet, Journal of Geophysical Research (Space Physics) **119**, 131 (2014).
[22] *Saas-Fee Advanced Course 24: Plasma Astrophysics* (1994).
[23] D. B. Melrose, Maser pulse emission mechanisms, in *Pulsars: 13 Years of Research on Neutron Stars*, Vol. 95, edited by W. Sieber and R. Wielebinski (1981) pp. 133–139.
[24] Y.-P. Yang and B. Zhang, Bunching Coherent Curvature Radiation in Three-dimensional Magnetic Field Geometry: Application to Pulsars and Fast Radio Bursts, The Astrophysical Journal **868**, 31 (2018), arXiv:1712.02702 [astro-ph.HE].
[25] A. J. Cooper and R. A. M. J. Wijers, Coherent curvature radiation: maximum luminosity and high-energy emission, Monthly Notices of the Royal Astronomical Society **508**, L32 (2021), arXiv:2108.07818 [astro-ph.HE].
[26] P. L. Pritchett, Relativistic electron production during guide field magnetic reconnection, Journal of Geophysical Research (Space Physics) **111**, A10212 (2006).
[27] E. A. Jackson, A new pulsar atmospheric model. I. Aligned magnetic and rotational axes., The Astrophysical Journal **206**, 831 (1976).
[28] I. Contopoulos, J. Pétri, and P. Stefanou, Hybrid numerical simulations of pulsar magnetospheres, Monthly Notices of the Royal Astronomical Society **491**, 5579 (2020), arXiv:1909.13504 [astro-ph.HE].
[29] G. I. Melikidze, J. A. Gil, and A. D. Pataraya, The Spark-associated Soliton Model for Pulsar Radio Emission, The Astrophysical Journal **544**, 1081 (2000), arXiv:astro-ph/0002458 [astro-ph].
[30] A. V. Bilous, J. M. Grießmeier, T. Pennucci, Z. Wu, L. Bondonneau, V. Kondratiev, J. van Leeuwen, Y. Maan, L. Connor, L. C. Oostrum, E. Petroff, J. P. W. Verbiest, D. Vohl, J. W. McKee, G. Shaifullah, G. Theureau, O. M. Ulyanov, B. Cecconi, A. H. Coolen, S. Corbel, S. Damstra, H. Dénes, J. N. Girard, B. Hut, M. Ivashina, O. O. Konovalenko, A. Kutkin, G. M. Loose, H. Mulder, M. Ruiter, R. Smits, P. L. Tokarsky, N. J. Vermaas, V. V. Zakharenko, P. Zarka, and J. Ziemke, Dual-frequency single-pulse study of PSR B0950+08, Astronomy and Astrophysics **658**, A143 (2022), arXiv:2109.08500 [astro-ph.HE].
[31] M. Caleb, I. Heywood, K. Rajwade, M. Malenta, B. W. Stappers, E. Barr, W. Chen, V. Morello, S. Sanidas, J. van den Eijnden, M. Kramer, D. Buckley, J. Brink, S. E. Motta, P. Woudt, P. Weltevrede, F. Jankowski, M. Surnis, S. Buchner, M. C. Bezuidenhout, L. N. Driessen, and R. Fender, Discovery of a radio-emitting neutron star with an ultra-long spin period of 76 s, Nature Astronomy **6**, 828 (2022), arXiv:2206.01346 [astro-ph.HE].
[32] A. K. Singal and H. O. Vats, Giant-pulse Emission from PSR B0950+08, The Astronomical Journal **144**, 155 (2012), arXiv:1209.5093 [astro-ph.HE].
[33] S. B. Zhang, J. J. Geng, J. S. Wang, X. Yang, J. Kaczmarek, Z. F. Tang, S. Johnston, G. Hobbs, R. Manchester, X. F. Wu, P. Jiang, Y. F. Huang, Y. C. Zou, Z. G. Dai, B. Zhang, D. Li, Y. P. Yang, S. Dai, C. M. Chang, Z. C. Pan, J. G. Lu, J. J. Wei, Y. Li, Q. W. Wu, L. Qian, P. Wang, S. Q. Wang, Y. Feng, and L. Staveley-Smith, RRAT J1913+1330: an extremely variable and puzzling pulsar, arXiv e-prints , arXiv:2306.02855 (2023), arXiv:2306.02855 [astro-ph.HE].
[34] D. Li, P. Wang, W. W. Zhu, B. Zhang, X. X. Zhang, R. Duan, Y. K. Zhang, Y. Feng, N. Y. Tang, S. Chatterjee, J. M. Cordes, M. Cruces, S. Dai, V. Gajjar, G. Hobbs, C. Jin, M. Kramer, D. R. Lorimer, C. C. Miao, C. H. Niu, J. R. Niu, Z. C. Pan, L. Qian, L. Spitler, D. Werthimer, G. Q. Zhang, F. Y. Wang, X. Y. Xie, Y. L. Yue, L. Zhang, Q. J. Zhi, and Y. Zhu, A bimodal burst energy distribution of a repeating fast radio burst source, Nature (London) **598**, 267 (2021), arXiv:2107.08205 [astro-ph.HE].
[35] P. H. Diamond and M. Malkov, Dynamics of helicity transport and Taylor relaxation, Physics of Plasmas **10**, 2322 (2003).
[36] Z. B. Guo, P. H. Diamond, and X. G. Wang, Magnetic Reconnection, Helicity Dynamics, and Hyper-diffusion, The Astrophysical Journal **757**, 173 (2012).
[37] K. Nimmo, J. W. T. Hessels, M. P. Snelders, R. Karuppusamy, D. M. Hewitt, F. Kirsten, B. Marcote, U. Bach, A. Bansod, E. D. Barr, J. Behrend, V. Bezrukovs, S. Buttaccio, R. Feiler, M. P. Gawroński, M. Lindqvist, A. Orbidans, W. Puchalska, N. Wang, T. Winchen, P. Wolak, J. Wu, and J. Yuan, A burst storm from the repeating FRB 20200120E in an M81 globular cluster, Monthly Notices of the Royal Astronomical Society **520**, 2281 (2023), arXiv:2206.03759 [astro-ph.HE].